analytical chemistry

Article

pubs.acs.org/ac

Analysis of DNA Binding and Nucleotide Flipping Kinetics Using Two-Color Two-Photon Fluorescence Lifetime Imaging Microscopy

Tom Robinson,[†,#] Prashant Valluri,[‡] Gordon Kennedy,[§] Alessandro Sardini,[∥] Christopher Dunsby,[§] Mark A. A. Neil,[†,§] Geoff S. Baldwin,[†,⊥] Paul M. W. French,*[,†,§] and Andrew J. de Mello*[,†]

[†]Institute of Chemical Biology, Department of Chemistry, Imperial College London, London SW7 2AZ, U.K.

[‡]Institute of Materials and Processes, Sanderson Building, School of Engineering, University of Edinburgh, King's Buildings, Edinburgh EH9 3JL, U.K.

[§]Photonics Group, Department of Physics, Imperial College London SW7 2AZ, U.K.

[∥]MRC Clinical Sciences Centre, Imperial College London, Hammersmith Hospital Campus, London W12 0NN, U.K.

[⊥]Division of Molecular Biosciences, Exhibition Road, London, SW7 2AZ, U.K.

Supporting Information

ABSTRACT: Uracil DNA glycosylase plays a key role in DNA maintenance via base excision repair. Its role is to bind to DNA, locate unwanted uracil, and remove it using a base flipping mechanism. To date, kinetic analysis of this complex process has been achieved using stopped-flow analysis but, due to limitations in instrumental dead-times, discrimination of the "binding" and "base flipping" steps is compromised. Herein we present a novel approach for analyzing base flipping using a microfluidic mixer and two-color two-photon (2c2p) fluorescence lifetime imaging microscopy (FLIM). We demonstrate that 2c2p FLIM can simultaneously monitor binding and base flipping kinetics within the continuous flow microfluidic mixer, with results showing good agreement with computational fluid dynamics simulations.

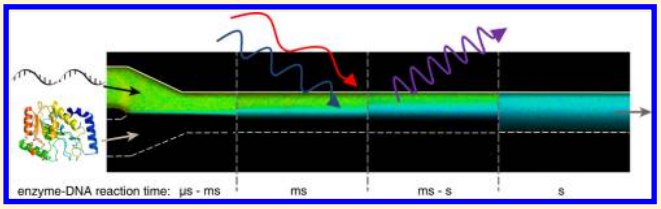

The detection and monitoring of biological processes provides an important means to study mechanistic and functional behavior at many different levels. Herein we address two key challenges in such studies, namely the rapid detection of fluorescence changes in kinetic measurements and the imaging of biological molecules that normally require deep ultraviolet excitation (and are therefore not detectable using conventional visible and near-UV spectroscopies).

Rapid kinetic analysis methods have a distinguished history in the biochemical sciences.[1,2] Surprisingly, the principal techniques of stopped-flow and quench-flow analysis, which are commonly used to study enzyme activity and conformational transitions, have not significantly changed during the last 50 years. The key limitation in both methods is the dead time associated with reagent mixing, which ultimately limits temporal resolution to approximately 1 ms. Shorter time scales can in principle be accessed through relaxation techniques such as the temperature jump method, but these are ill-suited to enzymatic processing, where enzyme and substrate must be kept separate prior to measurement.[1]

Microfluidic systems are convenient environments in which to perform kinetic studies on short time scales due to the ability to mix multiple reagent streams in a rapid and controllable fashion. Moreover, they are especially attractive for the study of biological processes due to their low sample/reagent requirements.[3] To this end, a range of microfluidic mixers operating within low Reynold's number regimes (and relying on diffusive mixing of reagents) have been used for the quantitative analysis of a variety of reactive systems.[4,5] Such devices can be readily calibrated and analyzed using computational fluid dynamics (CFD), and a number of recent studies have demonstrated that fluorescence lifetime imaging (FLIM) can provide a robust experimental readout of both fluid dynamics[6,7] and molecular kinetics[8] in such systems. For example, Matthews and co-workers recently utilized a simple Y-mixer to extract chemical rate constants by comparing time-resolved FLIM data with numerical simulations.[9]

Herein we report the use of microfluidic mixing and two-color two-photon (2c2p) FLIM to study the DNA repair enzyme uracil DNA glycosylase (UNG) due to its fundamental importance in maintaining DNA fidelity.[10] UNG is an initiator in the base excision repair (BER) pathway and also prevents mutagenesis by eliminating non-native uracil from DNA through cleavage of the N-glycosidic bond to leave an apyrimidinic (AP) site. This AP site is then processed by the remainder of the BER machinery. Specifically, an AP endonuclease cleaves the DNA backbone, a deoxyribophosphodiesterase removes the remaining ribosyl sugar from the 5′ phosphate, and a DNA polymerase and ligase fill and seal the gap.[11] UNG, like many DNA glycosylases, exploits the structural transition known as nucleotide flipping to gain access to the interior of the DNA helix and catalyze the removal of the unwanted base.[12] Despite being discovered two

Received: July 22, 2014
Accepted: September 28, 2014
Published: September 28, 2014

decades ago,[13] the precise molecular mechanism that underlies nucleotide flipping remains unclear. Due to the dynamic nature of nucleotide flipping, kinetic studies are desirable to interrogate the conformational transitions required, but conventional stopped-flow methodologies are limited in their ability to resolve such fast events.[14] For this reason, we propose a novel methodology incorporating continuous flow microfluidics that is able to simultaneously monitor DNA binding and nucleotide flipping by UNG.

Uracil lesion recognition by UNG is a two-step process in which the enzyme first binds the DNA and then flips the base into its active site. Significantly, it has been demonstrated that these two processes can be monitored independently. Binding can be monitored by labeling the DNA with extrinsic fluorophores and monitoring variations in fluorescence anisotropy.[14−16] Conversely, nucleotide flipping can be monitored by placing the fluorescent base analogue 2-aminopurine (2-AP) adjacent to the flipped uracil base.[17] These two signals can be used to contemporaneously monitor these events in sequence.[14]

The development of a microfluidic platform for studying UNG presents several challenges. While the hexachlorofluorescein (HEX) label commonly used to monitor DNA binding can be excited in the visible region of the electromagnetic spectrum (e.g., using pulsed diode lasers, using a fiber-laser pumped super continuum source to implement FLIM, or using an ultrafast Ti:sapphire laser for two photon excitation), the 2-AP base analogue used to probe nucleotide flipping can only be excited using ultraviolet radiation at wavelengths below the limit for two photon excitation using conventional Ti:sapphire lasers. To address this challenge, we propose the implementation of 2c2p FLIM,[18] which is able to excite fluorophores at wavelengths down to 300 nm with a greater efficiency than three-photon excitation.

EXPERIMENTAL SECTION

DNA and protein preparation. Synthetic oligonucleotides were synthesized by Eurogentec (Liège, Belgium). Their sequences are reported in Table 1, where U, P, and H indicate the positions of uracil, 2-AP, and HEX, respectively. Both 1U and 2U contain uracil and are tagged with HEX at the 5′ end via a flexible carbon linker. In addition, 2U also contains the base analogue 2-AP to allow detection of nucleotide flipping. In single stranded DNA, charge transfer from 2-AP to adenine is much more efficient than to other bases.[19] UNG is known to bind single stranded DNA as well as double stranded DNA,[15] and thus, since 2-AP is positioned adjacent to adenine in 2U, a significant change in fluorescence will be observed when the stacking is disrupted by UNG interaction.[15,17]

Table 1. Oligonucleotides Containing HEX and 2-AP Labels

Abbreviation	Sequence
1U	5′-(**H**)-GAC-TAA-UAA-TGA-CTG-CG-3′
2U	5′-(**H**)-GAC-TA**P**-UAA-TGA-CTG-CG-3′

HSV-1 UNG mutant (D88N/H210N) was purified and stored as previously described.[16] Wild-type UNG shows catalytic behavior, rapidly initiating base cleavage and subsequent dissociation. In the current studies, the inactive mutant was used to allow observation of binding in the absence of uracil removal.[16] This mutant has both of its catalytic residues mutated to Asn (asparagine) so that the DNA remains tightly bound to the substrate when uracil is flipped into the active site. Solutions of DNA and UNG were prepared in a buffer of 50 mM Tris pH 8.0, 1 mM EDTA, 150 mM NaCl and filtered before use with a 0.2 μm pore size filter to prevent introduction of particulates into the microfluidic system. All experiments were conducted at 25 °C.

Time-resolved measurements of HEX within DNA. Fluorescence lifetime decay profiles in solution were measured using a custom-built time-resolved fluorometer.[20] Specifically, HEX was excited using a pulsed fiber-laser-pumped supercontinuum source (SPC-400, Fianium, Southampton, U.K.) providing ultrashort pulses at 535 nm. Fluorescence decays were recorded at 550 nm with at least 10,000 counts being collected in the time-bin of maximum intensity. Excitation and emission spectra of HEX can be found in Figure S1 in the Supporting Information. An instrument response function (IRF) was measured using a scattering solution of colloidal silica (LUDOX, Sigma-Aldrich, U.K.). Analysis of the fluorescence decay profiles was performed using a TRFA Advanced Data Processor (SSTC, Minsk, Belarus).

Multiphoton FLIM. Multiphoton FLIM was performed using an inverted confocal microscope (TCS SP5, Leica Microsystems GmbH, Germany) equipped with time correlated single photon counting (TCSPC) electronics and using a femtosecond pulsed Ti:sapphire laser (Mai Tai, Newport Spectra-Physics, CA, USA) as the light source. HEX fluorescence was excited using two photon excitation and femtosecond pulses at 750 nm focused into the sample using a 40× air objective lens. Fluorescence emission was collected between 525 and 600 nm and the IRF recorded using an 0.5 M solution of trans-4-[4-(dimethylamino)styryl]-1-methylpyridinium iodide (DASPI) in methanol. Analysis of the fluorescence decays was performed using SPImage software (Becker & Hickl GmbH, Germany).

2c2p fluorometer. A 2c2p fluorometer was implemented (Figure S2) as a step toward 2c2p excitation in a FLIM microscope. To achieve efficient 2c2p excitation, two photons of different wavelengths must spatially and temporally coincide within the sample, with optimal excitation being achieved when both beams have the same polarization. Significantly, 2c2p excitation events have similar absorption cross sections to conventional one-color two-photon (1c2p) excitation,[21] thus making absorption probabilities much higher than three-photon excitation. To this end, the output of a Ti:sapphire laser (Mai Tai, Spectra-Physics, CA, USA) was tuned to 900 nm and frequency doubled to 450 nm using a BBO crystal. The two wavelengths were spatially separated using a 580 nm dichroic (DC_1). The 900 nm wavelength radiation was then directed to a corner cube coated with gold and mounted on a linear translation stage (UTM PP1HL, Newport, CA, USA). This provides for a temporal delay of the 900 nm pulses to enable overlapping with the 450 nm pulses at the sample. Both beamlines incorporated half wave ($\lambda/2$) retarding plates to rotate their polarization. In addition, the 450 nm radiation was passed through a variable neutral density filter for power adjustment. Both beams were recombined at a second 580 nm dichroic (DC_2) and focused into a quartz cuvette using an achromatic doublet lens with a focal length of 55 mm (L_3). The effective excitation wavelength (λ_{eff}) is given by eq 1, where λ_1 and λ_2 are the two excitation wavelengths.

$$\frac{1}{\lambda_{eff}} = \frac{1}{\lambda_1} + \frac{1}{\lambda_2} \quad (1)$$

Accordingly, a combination of 900 and 450 nm radiation results in an effective excitation wavelength of 300 nm. Emission was collected at an angle of 90° to the excitation direction with a fast photomultiplier (PMH-100, Becker and Hickl GmbH, Germany) using a fused silica lens with a 60 mm focal length (L_4). Scattered excitation light was blocked using a 360/35 nm

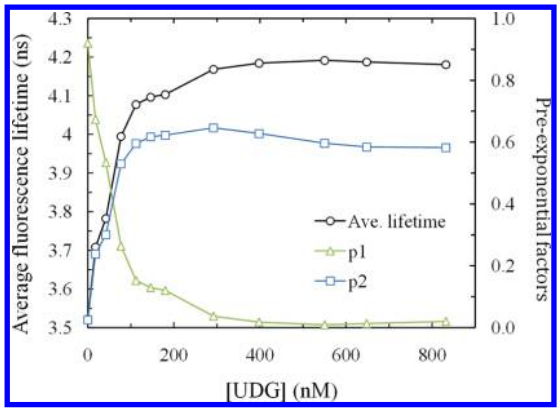

Figure 1. Time-resolved fluorescence spectroscopy of a fixed concentration of 1U (50 nM) showing the change in the pre-exponential factors and average fluorescence lifetime values with increasing amount of UNG. Here, p1 and p2 refer to the pre-exponentials of the 3.5 and 4.2 ns lifetimes respectively.

band-pass filter. All mirrors were coated with protected silver for high visible-to-IR reflectivity. For TCSPC measurements, the PMT was connected to a TCSPC card (SPC-830, Becker and Hickl GmbH, Germany). A quartz window positioned at the output of the Ti:sapphire laser reflected a small portion of the 900 nm radiation onto a fast photodiode (DET10A, Thorlabs GmbH). This signal was amplified (HSA-X-2-40, FEMTO Messtechnik GmbH, Germany) and connected to the TCSPC card for triggering. Detailed characterization of the system can be found in Figures S3, S4, and S5 in the Supporting Information.

2c2p fluorescence (lifetime) microscopy. For fluorescence microscopy using 2c2p excitation, two excitation beams were directed to the back port of an inverted epi-fluorescence microscope (IX71, Olympus, Japan) using a periscope (Figure S6). A fully reflective aluminum mirror inside the microscope directed the beams to a UV optimized 40× oil objective lens (UAPON, Olympus, Japan) to illuminate the sample. Fluorescence was collected via the same objective lenses and directed toward the PMT using a 400 nm dichroic mirror (DC_3). A UV fused silica lens with a 60 mm focal length (L_5) focused the light onto the photocathode of the PMT with excitation light being blocked using a 360/35 nm band-pass filter. The alignment and overlap of the two excitation spots was achieved using a test sample consisting of a 80 nm thick fluorescent polymer film. Alignment in the z-direction was made possible with a telescope (positioned in the 900 nm radiation path) consisting of two lenses (L_3, L_4) of focal lengths 35 and 63 mm, respectively, mounted on separate linear translation stages. Fluorescence images were built up by raster scanning the spots across the sample (in both the x and y directions) using a motorized stage (ScanIM, Märzhäuser GmbH, Germany). Control of the stage and collection of the signal from the PMT was performed using custom software written in the LabView graphical programming environment.

Microfluidic chip fabrication and operation. Planar microfluidic chips were made from polydimethysiloxane (PDMS) and glass using soft lithographic methods that have been described in detail elsewhere.[22] Briefly, a master mold was produced on a silicon wafer (where all feature heights were 100 μm) by exposing a negative photoresist layer (SU-8 50, MicroChem, MA, USA) to UV radiation. A structured PDMS layer was then formed by mixing oligomer and curing agent (Sylgard 184 Elastomer Kit, Dow Corning, MI, USA) at a ratio of 10:1 and pouring this mixture on top of the master. After curing at 65 °C for 5 h, the structured PDMS substrate was peeled off the master, and access holes punched through the PDMS using a biopsy punch (1.5 mm, Miltex, Germany). Microchannels were enclosed by bonding the structured PDMS layer to a glass coverslip in an air plasma oven (PDC-002, Harrick Plasma, NY, USA).

Reagents were delivered into microchannels via fluorinated ethylene propylene (FEP) tubing (Teflon FEB, Anachem, Luton, U.K.) inserted into the inlet reservoirs. The FEP tubing was then connected to 1 mL glass syringes (Hamilton Gastight 1000 series, Sigma-Aldrich, U.K.) via finger tights and polyetheretherketone (PEEK) tubing (Sigma-Aldrich, U.K.). Hydrodynamic flow was generated using precision syringe pumps (IITC Life Science, CA, USA) and the outlet tubing placed into a waste reservoir. Prior to experiments, 0.1 wt % n-dodecyl-β-D-maltoside (DDM) in water was flowed through the channels for 15 min at 3 μL/min. Such a pretreatment was shown to be efficient in minimizing DNA and protein adsorption to channel surfaces.[23]

Computational fluid dynamic simulations. CFD simulations were performed using ANSYS CFX (Canonsburg, PA, USA), as previously detailed.[7] In brief, the software simultaneously solves the 3D conservation equations of momentum, continuity, and advection-reaction-diffusion of species that describe both fluid flow and reaction using the finite volume method. Further details of the simulation conditions and the implemented boundary conditions are provided in the Supporting Information. To simulate the reaction between UNG and DNA, additional rate terms were extracted from literature data reported by Bellamy and co-workers.[14] The geometry of the computational domain was designed to closely match the microchannel dimensions of the Y-mixer used in the current experiments. The finite volume element mesh was created inside the geometry by setting the maximum cell length to less than 1/20th of the smallest feature. To simulate quenching of fluorescein fluorescence, the mesh had a maximum cell length of 5 μm and a total of 1,754,264 elements. Molecular diffusion coefficients of 2×10^{-9} m^2 s^{-1} ($D_{\text{NaI-Wat}}$) for sodium iodide and 6×10^{-10} m^2 s^{-1} ($D_{\text{Fl-Wat}}$) for fluorescein (both in water) were used in all simulations. In all cases a solution was found within less than 200 iterations and in less than 1 h using a dual-core 2.13 GHz Intel© processor. Two computational domains were required to simulate the reaction between UNG and DNA in the Y-mixer. The first had a maximum cell length of 2.5 μm, a channel length of 2.5 cm, and a total of 2,317,396 elements. The second had a maximum cell length of 5 μm, a channel length of 4 cm, and a total of 4,086,724 elements. Accordingly, the reaction at 4 cm could be simulated with reduced resolution, while reactions at 0, 1.5, and 2.5 cm could be simulated with high resolution. The molecular diffusion coefficient of 2U in water ($D_{\text{2U-Wat}}$) was assumed to be 4×10^{-11} m^2 s^{-1} and that of UNG ($D_{\text{UNG-Wat}}$) to be 7×10^{-11} m^2 s^{-1}. In all cases a solution was found in less than 250 iterations and in less than 5 h using a dual-core 2.13 GHz Intel© processor.

RESULTS AND DISCUSSION

Time-resolved measurements of UNG-DNA binding. UNG-DNA binding can be monitored by assessing the change in the fluorescence polarization anisotropy of the HEX label. Such variations in anisotropy are due an increase in rotational diffusion times as the mass of the fluorophore complex increases.[24,25] To assess whether fluorescence decay time variations can be used to monitor UNG-DNA binding, fluorescence

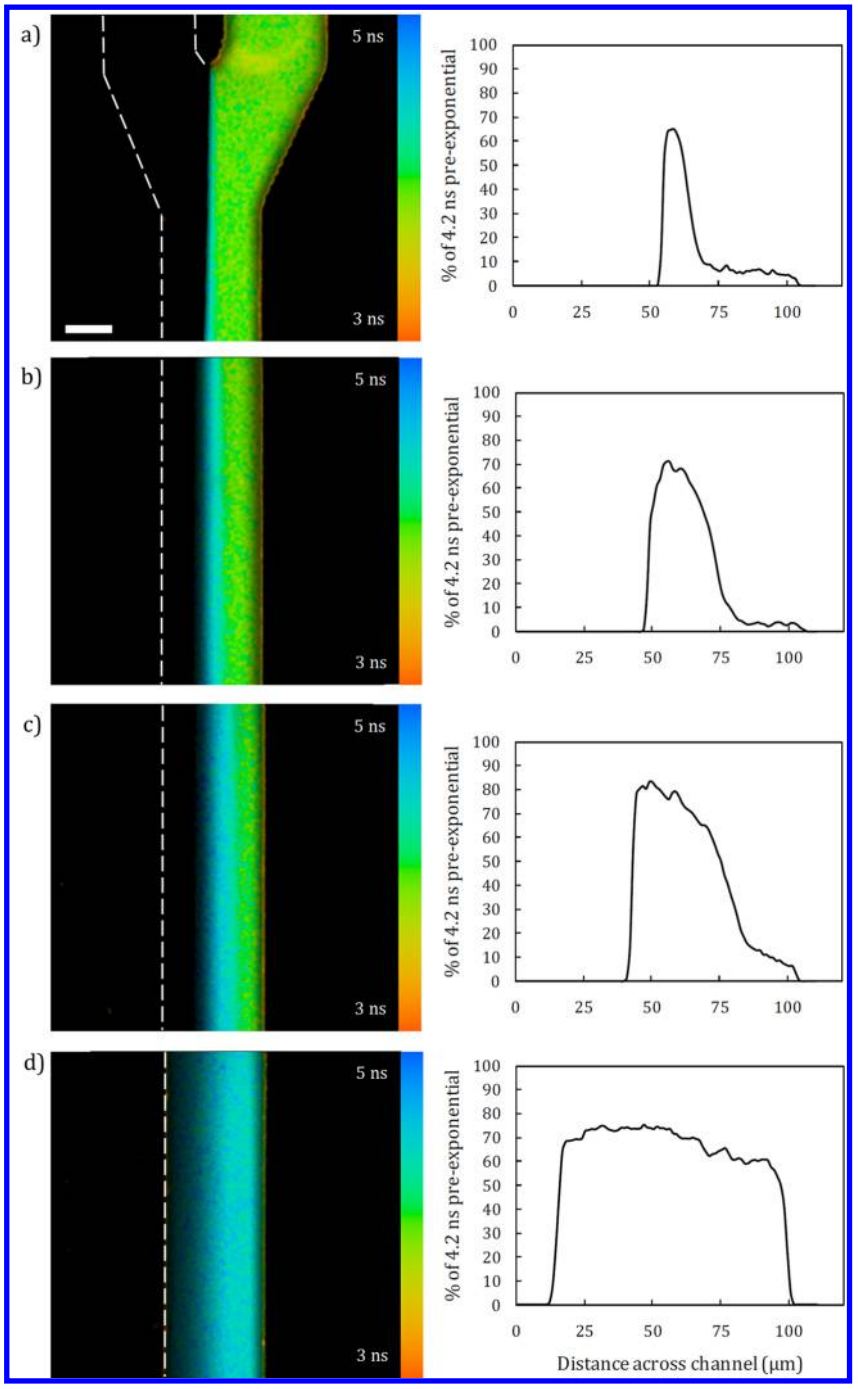

Figure 2. FLIM analysis of UNG-DNA binding in a microfluidic mixer. FLIM images using a single exponential model (left-hand panels) at (a) 0 mm, (b) 1 mm, (c) 2.5 mm, and (d) 10 mm corresponding to average residence times of 108, 540, 1350, and 5400 ms respectively. Scale bar: 50 μm. The right-hand panels show line profiles of the % bound DNA derived from the 4.2 ns pre-exponential using a double exponential model.

decay profiles (at 535 nm excitation) originating from solutions containing increasing amounts of UNG and a fixed concentration (50 nM) of 1U oligonucleotide were measured. Previously, the fluorescence decay of HEX has been reported to be well-described by a single exponential decay law in the unbound state, but any change upon enzyme binding has yet to be explored.[25] In the current experiments, all fluorescence decay profiles were globally analyzed using a double exponential decay model with fixed lifetime values of 3.5 and 4.2 ns. These values represent the "free" and "bound" fluorophore populations in the sample. Figure 1 illustrates the variation of both the average fluorescence lifetime and the magnitude of the pre-exponential factors as a function of UNG concentration. It is observed that as the amount of (bound) UNG is increased, the pre-exponential factor (or amplitude) of the shorter lifetime component decreases and the pre-exponential factor of the longer component increases. Accordingly, the average fluorescence decay time is seen to increase from 3.5 to 4.2 ns (with reduced χ^2 values between 1.38 and 1.41). The physical interpretation of such a change is most likely due to the switching-off of nonradiative deactivation caused by the enzyme changing the conformation of the DNA and hence the rigidity of the linker moiety. Such a dependence of fluorescence decay times on the fluorophore rigidity has been noted previously.[26,27]

dx.doi.org/10.1021/ac502732s | *Anal. Chem.* 2014, 86, 10732−10740

Quantitative fluorescence polarization anisotropy, which is commonly used for such measurements of binding, generally assumes that there is no change in the fluorescence lifetime on binding. Since a change in the fluorescence lifetime is clearly observed in the current system, measurement of fluorescence decay time variations represents a more appropriate method of monitoring the binding process.

With the aim of measuring such signals within a microfluidic environment, 3 μM of oligonucleotide 1U and 20 μM UNG were introduced into the inlet channels of the Y-mixer (50 μm high and 100 μm wide) at a flow rate of 0.25 μL/min. Microfluidic Y-mixers have been extensively studied both experimentally and theoretically.[5,28−31] In particular they can be used to measure reaction rates that would otherwise be impossible using conventional stopped-flow techniques.[5] Fluorescence lifetime images were acquired at 0, 1, 2.5, and 10 mm from the point of confluence (corresponding to average residence times of 108, 540, 1350, and 5400 ms) using multiphoton FLIM microscopy, and resulting fluorescence decay profiles were fitted to a single exponential decay model (Figure 2). As expected, the extracted decay times increase as the two species diffuse and bind near the center of the microchannel. Fluorescence lifetime images were then fitted to a double exponential decay model with fixed fluorescence lifetimes of 3.5 and 4.2 ns (using the values from the bulk solution measurements). The generated line profiles (Figure 2) allow direct quantification of the bound population via assessment of the pre-exponential factor of the longer lifetime component. Therefore, measurements of the fluorescence lifetime can be used to directly monitor enzyme binding to DNA. Unfortunately, observation of base flipping using the current setup requires excitation of the 2-AP base analogue via three photon excitation, which is problematic due to the low excitation cross-section.[26] Accordingly, it was decided to develop a 2c2p source to facilitate excitation of 2-AP in the UV region of the electromagnetic spectrum; a markedly more efficient process than three photon excitation.

2c2p fluorometer. Fluorescence from a control sample of 5 mM tryptophan (Sigma-Aldrich, UK) in pH 7.4 PBS buffer was used to assess the performance of the system (Figure S7). First, multiphoton excitation (1c2p) was performed using 3.3 mW at 450 nm and an acquisition time of 1 s. The emission spectra of tryptophan can be found in Figure S1. The resulting decay profiles were analyzed using a single exponential decay model, yielding a fluorescence lifetime of 2.55 ns with a reduced χ^2 of 1.08 (Figure S7a), which is consistent with literature values.[32] Fluorescence was then acquired using three photon (1c3p) excitation with an average power of 50 mW at 900 nm (Figure S7b). It should be noted that the lower photon detection rates necessitated an acquisition time of 30 min. Fluorescence decay profiles were analyzed using a single exponential decay model and yielded a lifetime of 2.62 ns with a reduced χ^2 of 1.17. This increase in fluorescence lifetime is most likely due to the increased background signal collected during the 30 min acquisition time. Finally, 2c2p excitation was performed using 3.3 mW at 450 nm and 50 mW at 900 nm with an integration time of 1 s (Figure S7c). Addition of the 900 nm beam resulted in a 2.2-fold improvement in the obtained fluorescence signal compared to 1c2p excitation and a 4300-fold improvement compared with 1c3p excitation. Again the resulting fluorescence decay profiles were analyzed using a single exponential model, which yielded a fluorescence lifetime of 2.49 ns with a χ^2 of 1.21. This result confirms that the system is capable of performing fluorescence lifetime values using 2c2p excitation.

2c2p fluorescence (lifetime) microscopy. To assess the imaging capability of the 2c2p fluorescence microscope, fluorescence intensity images of tryptophan powder on a coverslip were acquired using an analogue photomultiplier tube (H8249-102, Hamamatsu Photonics, Japan). For the first region scanned (Figure 3a), the powers of the 450 and 900 nm laser

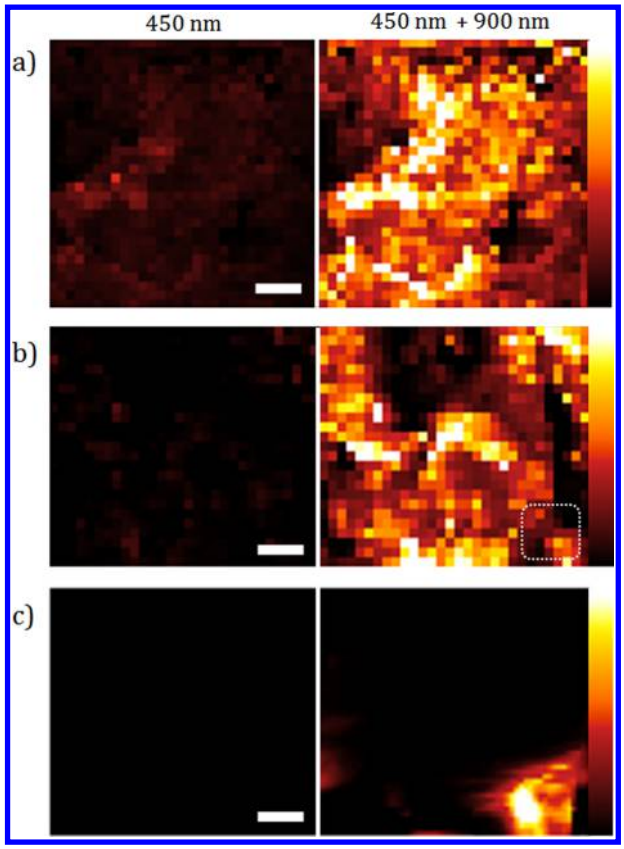

Figure 3. Fluorescence intensity images of tryptophan powder with 1c2p (left) and 2c2p (right) excitation. (a) First region with 10 μm step size. Scale bar: 50 μm. (b) Second region with 10 μm step size. Scale bar: 50 μm. (c) Scan of dashed area in second region with 1 μm step size. Scale bar: 10 μm.

beams were 1 and 48 mW, respectively. It is observed that the fluorescence intensity improves 4-fold with the addition of the 900 nm beam. For the second region (Figure 3b), the 450 nm power was reduced to 0.33 mW with the 900 nm power held at 48 mW. By increasing the 900 nm/450 nm ratio, 1c2p excitation is suppressed and the fluorescence intensity improves 28-fold with the addition of the 900 nm beam. The dashed area highlighted in Figure 3b was then imaged using the same experimental conditions and scanned with a 1 μm step size for improved resolution (Figure 3c). It should be noted that without the 900 nm beam, negligible fluorescence was observed in this area and for all regions negligible emission was observed when the sample was excited by 900 nm radiation alone.

To perform FLIM, the analogue photomultiplier was replaced with a photon-counting photomultiplier (PMH-100, Becker and Hickl GmbH, Germany) for TCSPC detection. To demonstrate 2c2p FLIM, the instrument was first applied to the analysis of *ex vivo* fixed mouse skin tissue. Figure 4 shows the 2c2p excited autofluorescence images acquired 12 μm below the surface of an

dx.doi.org/10.1021/ac502732s | *Anal. Chem.* 2014, 86, 10732−10740

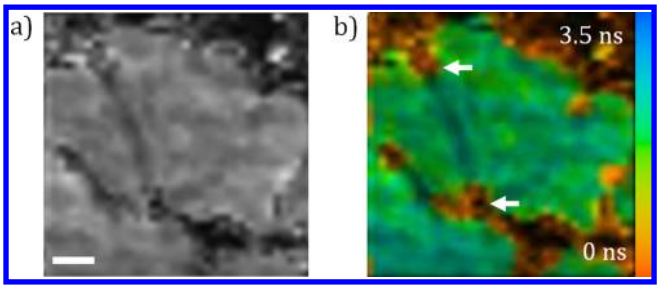

Figure 4. 2c2p excited autofluorescence of unstained mouse tissue. a) Intensity image and b) lifetime image showing the mean fluorescence lifetime calculated from a fit to a double exponential decay model. White arrows indicate regions of collagen. Scale bar is 10 μm and the image intensities have been normalized.

unstained sample of mouse tissue using 0.55 mW at 450 nm and 50 mW at 900 nm. The time-integrated fluorescence intensity (Figure 4a) and fluorescence lifetime (Figure 4b) images are provided. When comparing the two images, additional contrast from the lifetime data is observed between the skin tissue and regions attributed to collagen (indicated by white arrows). Further details are available in Figure S8 the Supporting Information.

Validation of CFD using FLIM of the quenching of fluorescein by NaI. To ensure that the CFD simulations accurately mimic the operation of the Y-mixer, we compared simulation results with experimental measurements of the fluorescence quenching of fluorescein by NaI: a method that has previously been used to validate the efficacy of simulation studies.[7] A 50 μM fluorescein solution and a 625 mM NaI solution (both in water with a 500 mM Tris buffer at pH 8.3) were introduced into the inlet channels, each at a flow rate of 0.5 μL/min. FLIM data were acquired using 1c2p excitation (exciting at 900 nm) to provide optically sectioned imaging, and emission was collected using a 560/25 nm band-pass filter. The beam was scanned across the width of the microchannel in 2 μm steps (with a 1 s acquisition time per step) at positions 0, 0.25, 0.5, and 2 cm from the point of confluence (corresponding to average residence times of 15 ms, 375 ms, 750 ms, and 3 s). The spatial distribution of the NaI was then calculated from the fluorescence lifetime of the fluorescein and compared to the simulated values (Figure 5).[7] A 3-D rendering of the CFD simulation at the point of confluence is provided in Figure S9. The good agreement between the two data sets indicates that CFD can be used to simulate UNG-DNA diffusion and reaction.

Simultaneous detection of binding and base flipping. Prior to use in the Y-mixer, the fluorescence decays of 2-AP within 2U were measured in a multiwell plate using 2c2p excitation. Unwanted 1c2p excitation results in the excitation of the 7 tryptophan and 5 tyrosine residues within UNG; therefore, the output of the Ti:sapphire laser was tuned to 950 nm, resulting in a doubled wavelength of 475 nm from the BBO crystal. This enhances 2-AP excitation, since the effective excitation wavelength is shifted to 317 nm. To further suppress any 1c2p excitation, the power of the 475 nm beam was maintained below 1.5 mW and the power of the 950 nm beam was maintained at 51 mW. Fluorescence decays were collected from 5 μM 2U DNA for 60 s and then repeated after the addition of UNG at an excess concentration of 25 μM (Figure 6). Resulting fluorescence decays were analyzed using a double exponential decay model. The average fluorescence lifetime increased from 720 ps (reduced χ^2 = 1.24) to 1.64 ns (reduced χ^2 = 1.19) with addition of UNG. We attribute this variation to the fluorophore being quenched to a lesser extent when the adjacent base is flipped by the enzyme.

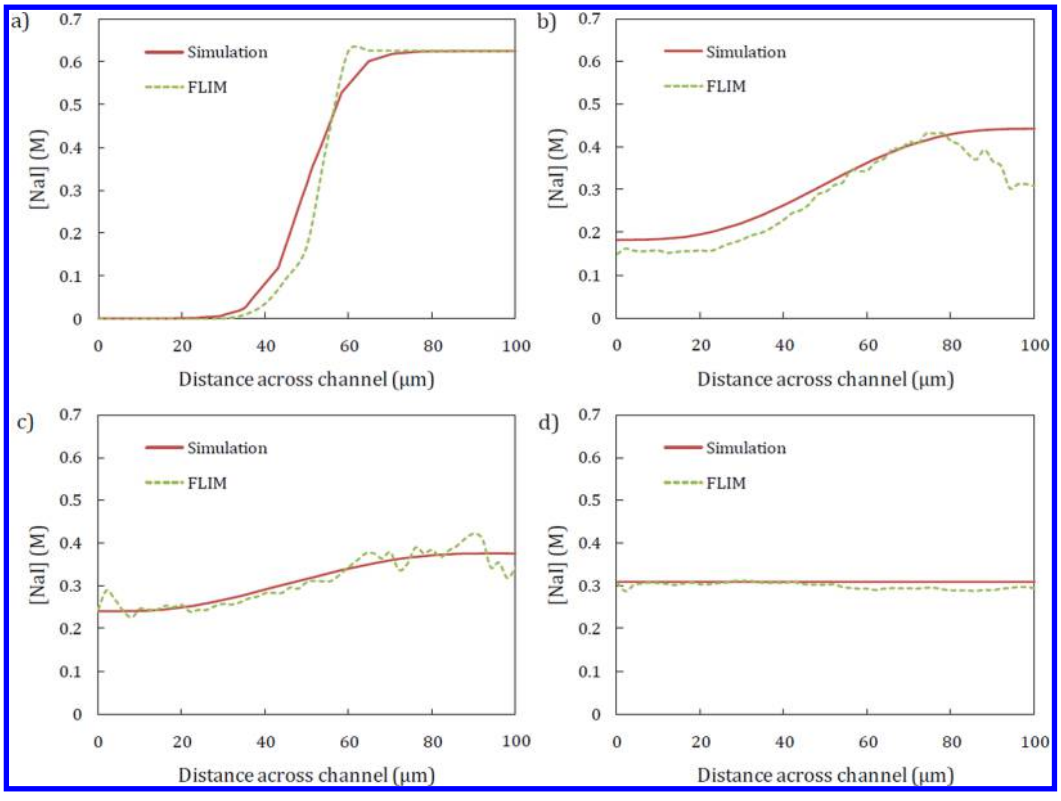

Figure 5. Line profiles of the concentration of NaI obtained from CFD simulations and FLIM at positions (a) 0 cm, (b) 0.25 cm, (c) 0.5 cm, and (d) 2 cm down the Y-mixer corresponding to average residence times of 15 ms, 375 ms, 750 ms, and 3 s, respectively.

dx.doi.org/10.1021/ac502732s | Anal. Chem. 2014, 86, 10732−10740

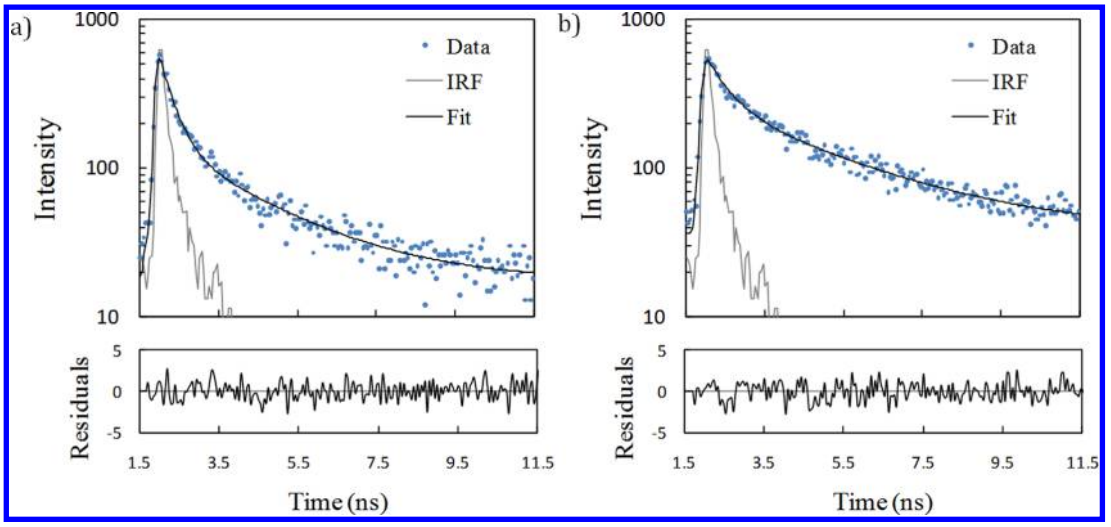

Figure 6. Time-resolved fluorescence of 2-AP within DNA excited using 2c2p, (a) without UNG and (b) with 25 μM UNG.

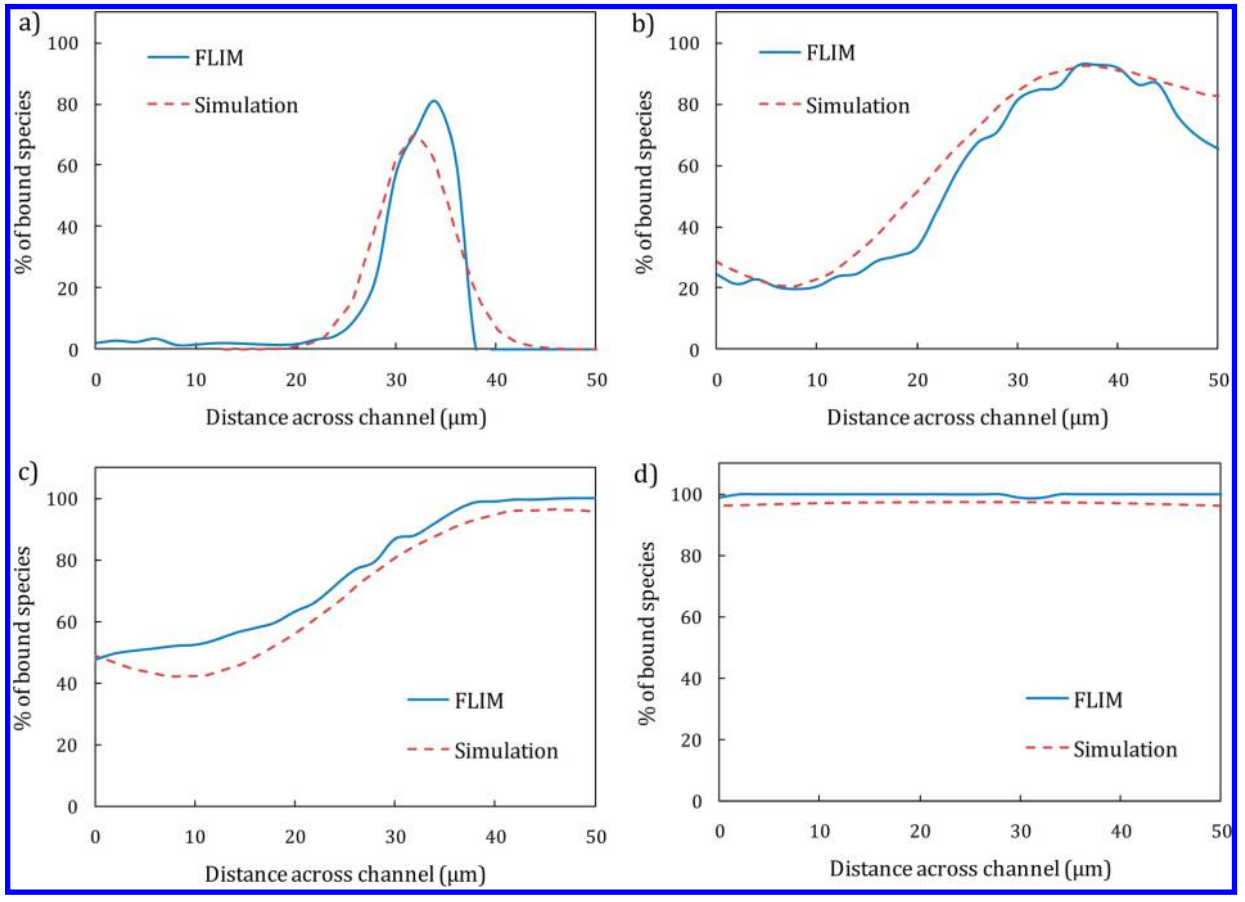

Figure 7. Line profiles of the percentage of bound species measured experimentally and simulated at positions (a) 0 cm, (b) 0.25 cm, (c) 1.5 cm, and (d) 4 cm from the point of confluence, corresponding to average residence times of 15 ms, 375 ms, 2.25 s, and 6 s, respectively.

2U DNA (10 μM) and UNG (45 μM) solutions were then introduced into the Y-mixer at individual flow rates of 0.5 μL/min. Excitation beams were scanned across the width of the channel (at the center of the channel to minimize any signal from surface bound DNA) in 1 μm steps at 0, 0.25, 1.5, and 4 cm from the junction (corresponding to average residence times of 15 ms, 375 ms, 2.25 s, and 6 s). This was repeated using a 560/20 nm emission filter for HEX and a 360/35 nm emission filter for 2-AP (excitation and emission spectra for HEX and 2-AP can be found in Figure S1). The acquisition time per step was 1 s for HEX and 10 s for 2-AP. CFD simulations were also performed using the same concentrations and flow rates. The reaction scheme is shown in Scheme 1, where E represents the enzyme, S the substrate, ES the bound species, and ES* the flipped species. The binding rate (k_1) was set to 1.54×10^8 M^{-1} s^{-1}, and the base flipping rate (k_2) was set to 670 s^{-1}. These values were extracted from previous data reported by Bellamy and co-workers measured via

dx.doi.org/10.1021/ac502732s | *Anal. Chem.* 2014, 86, 10732−10740

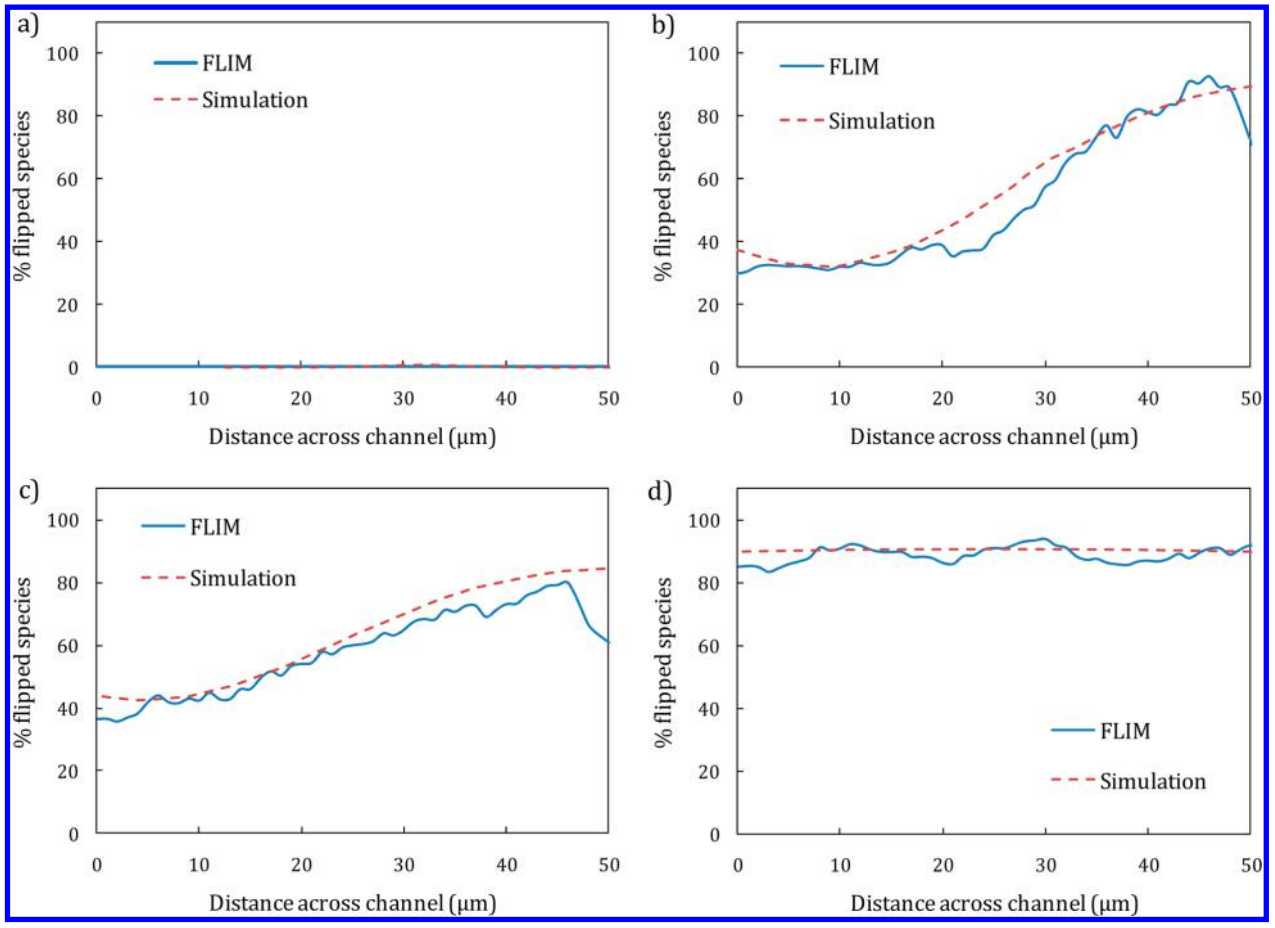

Figure 8. Line profiles of the percentage of flipped species measured experimentally and simulated at positions (a) 0 cm, (b) 0.25 cm, (c) 1.5 cm, and (d) 4 cm from the point of confluence, corresponding to average residence times of 15 ms, 375 ms, 2.25 s, and 6 s, respectively.

stopped-flow techniques.[14] Here, k_{-1} was omitted, as UNG was in excess.

$$E + S \overset{k_1}{\rightarrow} ES \overset{k_2}{\rightarrow} ES^* \qquad \text{(Scheme 1)}$$

For the analysis of the fluorescence decay profiles from HEX, a double exponential decay model was used with fluorescence lifetime values fixed at 3.5 and 4.2 ns, to represent the unbound and bound populations, respectively. The percentage of the bound component across the channel width was then overlaid with the expected percentage of bound species from the simulation. The resulting line profiles at the four different positions are illustrated in Figure 7 and show good agreement between the experimental and simulated data. Variations in the percentage of bound species at a given lateral position are likely to arise from fabrication defects that are unaccounted for in the simulation.

A double exponential model was used to fit the fluorescence decays of 2-AP within the mixer. The fluorescence lifetime values were fixed at 720 ps and 1.64 ns (i.e., the mean fluorescence lifetime values measured in solution for the flipped and nonflipped species). The percentage of the flipped component across the channel width was then overlaid with the percentage of flipped species concentration from the simulation (Figure 8). As with the HEX data in Figure 7, the line profiles are in excellent agreement with each other. At 0 cm, both data sets report less than 1% of the flipped species. At the same position, the HEX data reports up to 80% of bound DNA. These data show that the current experimental system is able to resolve the binding and base flipping processes between 0 and 25 μs. It should be noted that the 2-AP data do not report 100% of the flipped species at 4 cm, since the binding reaction is reversible.

CONCLUSIONS AND OUTLOOK

We have presented a novel method for monitoring a two-step enzyme−DNA reaction using a 2c2p FLIM microscope and a microfluidic mixing device. The good agreement between the experimental and simulated data for both the binding and flipping processes validates the experimental technique. It is noted that, for the current biological system, the rate constants used in the simulation were extracted from the literature. Nevertheless, the study of reactions with unknown kinetic parameters can be achieved by comparing a series of simulations (with different rates) with the experimental data. Indeed, this method was demonstrated by Matthews et al. in the measurement of the kinetics of a simple chemical reaction.[9]

With an increase in access to microfluidic technology and the continuing cost reductions of optical components, we believe that this method will become a valuable tool for investigating the kinetics of biological processes. In principle this technique could be extended to other biological systems such as protein−protein binding, single molecule DNA studies, or drug−lipid interactions. While the current setup is based on monitoring fluorescence, it does not necessarily require the use of fluorescent labels, as intrinsic autofluorescence can be monitored using the 2c2p excitation. This opens up the possibility of

dx.doi.org/10.1021/ac502732s | Anal. Chem. 2014, 86, 10732−10740

investigating other fast enzymatic reactions or even fast protein folding events. Finally, the use of excitation radiation in the visible and near-IR results in significantly reduced photodamage within biological samples compared to UV excitation and affords increased light penetration of biological tissue. Accordingly, we expect that 2c2p excitation will be highly useful in exciting tissue autofluorescence for biomedical research.

■ ASSOCIATED CONTENT

Supporting Information

Details of the equations, boundary conditions, and results of the CFD simulations. Characterization and setup of the 2c2p fluorometer. Time-resolved fluorescence of free tryptophan excited with 1c2p, 1c3p, and 2c2p. Schematic of the 2c2p microscope setup. Details of the 2c2p FLIM analysis of skin tissue. Excitation and emission spectra of tryptophan, HEX, and 2-AP. This material is available free of charge via the Internet at http://pubs.acs.org.

■ AUTHOR INFORMATION

Corresponding Authors

*(P.M.W.F.) E-mail: paul.french@imperial.ac.uk.
*(A.J.M.) E-mail: andrew.demello@chem.ethz.ch.

Present Address

#(T.R.) Max Planck Institute of Colloids and Interfaces, Department of Theory and Bio-Systems, Am Muehlenberg 1, Potsdam-Golm, 14476, Germany.

Author Contributions

The manuscript was written through contributions of all authors. All authors have given approval to the final version of the manuscript.

Notes

The authors declare no competing financial interest.

■ ACKNOWLEDGMENTS

T.R. would like to acknowledge a Ph.D. studentship from the UK Engineering and Physical Sciences Research Council (EPSRC) through the Institute of Chemical Biology at Imperial College London. A.J.M. would like to acknowledge partial support by the National Research Foundation of Korea (Global Research Laboratory Programme Grant K20904000004-10A0500-00410). P.F. and C.D. acknowledge partial support from the EPSRC (EP/F040202/1).

■ REFERENCES

(1) Fersht, A. *Structure and mechanism in protein science*; W. H. Freeman: New York, 1998.
(2) Gutfreund, H. *Kinetics for the Life Sciences*; Cambridge University Press: Cambridge, 1995.
(3) Knight, J. B.; Vishwanath, A.; Brody, J. P.; Austin, R. H. *Phys. Rev. Lett.* **1998**, *80*, 3863−3866.
(4) Kamholz, A. E.; Weigl, B. H.; Finlayson, B. A.; Yager, P. *Anal. Chem.* **1999**, *71*, 5340−5347.
(5) Baroud, C. N.; Okkels, F.; Ménétrier, L.; Tabeling, P. *Phys. Rev. E* **2003**, DOI: 10.1103/PhysRevE.67.060104.
(6) Benninger, R. K. P.; Hofmann, O.; McGinty, J.; Requejo-Isidro, J.; Munro, I.; Neil, M. A. A.; deMello, A. J.; French, P. M. W. *Opt. Express* **2005**, *13*, 6275−6285.
(7) Robinson, T.; Valluri, P.; Manning, H. B.; Owen, D. M.; Munro, I.; Talbot, C. B.; Dunsby, C.; Eccleston, J. F.; Baldwin, G. S.; Neil, M. A.; de Mello, A. J.; French, P. M. W. *Opt. Lett.* **2008**, *33*, 1887−1889.
(8) Benninger, R. K.; Hofmann, O.; Onfelt, B.; Munro, I.; Dunsby, C.; Davis, D. M.; Neil, M. A.; French, P. M.; de Mello, A. J. *Angew. Chem., Int. Ed. Engl.* **2007**, *46*, 2228−31.
(9) Matthews, S. M.; Elder, A. D.; Yunus, K.; Kaminski, C. F.; Brennan, C. M.; Fisher, A. C. *Anal. Chem.* **2007**, *79*, 4101−9.
(10) Lindahl, T. *Proc. Natl. Acad. Sci. U. S. A.* **1974**, *71*, 3649−3653.
(11) Seeberg, E.; Eide, L.; Bjoras, M. *Trends Biochem. Sci.* **1995**, *20*, 391−397.
(12) Roberts, R. J.; Cheng, X. *Annu. Rev. Biochem.* **1998**, *67*, 181−198.
(13) Klimasauskas, S.; Kumar, S.; Roberts, R. J.; Cheng, X. *Cell* **1994**, *76*, 357−369.
(14) Bellamy, S. R.; Krusong, K.; Baldwin, G. S. *Nucleic Acids Res.* **2007**, *35*, 1478−1487.
(15) Bellamy, S. R.; Baldwin, G. S. *Nucleic Acids Res.* **2001**, *29*, 3857−3863.
(16) Krusong, K.; Carpenter, E. P.; Bellamy, S. R.; Savva, R.; Baldwin, G. S. *J. Biol. Chem.* **2006**, *281*, 4983−4992.
(17) Stivers, J. T. *Nucleic Acids Res.* **1998**, *26*, 3837−3844.
(18) Quentmeier, S.; Denicke, S.; Gericke, K. H. *J. Fluoresc.* **2009**, *19*, 1037−1043.
(19) Rachofsky, E. L.; Osman, R.; Ross, J. B. A. *Biochemistry* **2001**, *40*, 946−956.
(20) Manning, H. B.; Kennedy, G. T.; Owen, D. M.; Grant, D. M.; Magee, A. I.; Neil, M. A.; Itoh, Y.; Dunsby, C.; French, P. M. W. *J. Biophotonics* **2008**, *1*, 494−505.
(21) Lakowicz, J. R.; Gryczynski, I.; Malak, H.; Gryczynski, Z. *Photochem. Photobiol.* **1996**, *64*, 632−5.
(22) Benninger, R. K.; Koç, Y.; Hofmann, O.; Requejo-Isidro, J.; Neil, M. A.; French, P. M. W.; de Mello, A. J. *Anal. Chem.* **2006**, *78*, 2272−8.
(23) Huang, B.; Wu, H.; Kim, S.; Zare, R. N. *Lab Chip* **2005**, *5*, 1005−1007.
(24) Grippon, S.; Zhao, Q.; Robinson, T.; Marshall, J. J.; O'Neill, R. J.; Manning, H.; Kennedy, G.; Dunsby, C.; Neil, M. A.; Halford, S. E.; French, P. M. W.; Baldwin, G. S. *Nucleic Acids Res.* **2011**, *39*, 2593−2603.
(25) Powell, L. M.; Connolly, B. A.; Dryden, D. T. F. *J. Mol. Biol.* **1998**, *283*, 947−961.
(26) Lakowicz, J. R. *Principles of Fluorescence Spectroscopy*, 3rd ed.; Springer: New York, 2006.
(27) de Mello, A. J.; Crystall, B.; Rumbles, G. *J. Colloid Interface Sci.* **1995**, *169*, 161−167.
(28) Ismagilov, R. F.; Stroock, A. D.; Kenis, P. J. A.; Whitesides, G.; Stone, H. A. *Appl. Phys. Lett.* **2000**, *76*, 2376−2378.
(29) Elder, A. D.; Matthews, S. M.; Swartling, J.; Yunus, K.; Frank, J. H.; Brennan, C. M.; Fisher, A. C.; Kaminski, C. F. *Opt. Express* **2006**, *14*, 5456−67.
(30) Desportesa, S.; Yatabeb, Z.; Baumlina, S.; Génota, V.; Lefèvrea, J.-P.; Ushikib, H.; Delairea, A. J.; Pansua, R. B. *Chem. Phys. Lett.* **2007**, *446*, 212−216.
(31) Batabyal, S.; Rakshit, S.; Kar, S.; Pal, S. K. *Rev. Sci. Instrum.* **2012**, *83*, 043113.
(32) Quentmeier, S.; Denicke, S.; Ehlers, J. E.; Niesner, R. A.; Gericke, K. H. *J. Phys. Chem. B* **2008**, *112*, 5768−5773.